Voltage Control of Four-Leg VSC for Power System Applications with Nonlinear and Unbalanced Loads

Juan Carlos Olives-Camps, *Student Member, IEEE,* Juan Manuel Mauricio, *Member, IEEE*
Manuel Barragán-Villarejo and Francisco Jesús Matas-Díaz

***Abstract*—Voltage source converters are presented as the key devices for the future massive integration of distributed renewable energy resources in the network. This paper presents a novel approach to control a three-phase four-leg voltage source converter for grid-forming operation. The objective of the controller is to generate a balanced three-phase voltage with a given amplitude and frequency at the point of common coupling. The proposed control algorithm works over the stationary axes. It is based on full state feedback law in combination with a resonant control loop tuned at the fundamental frequency in order to guaranty zero steady-state error on the voltage. The main advantage of the controller with respect to the classical cascade controllers is that this strategy is not modified depending on the type of load connected at the point of common coupling. Moreover, a systematic methodology to compute the controller gains is presented by solving an linear quadratic regulator problem that considers an extended model. This method guarantees small signal stability and provides active damping to the system. A laboratory testbed with different type of loads is used to validate and compare the proposed algorithm with the classical one. The experimental results demonstrate the effectiveness of the proposal by achieving low levels of harmonic distortion and imbalances in steady-state as well as a fast transient response.**

***Index Terms*—Four-leg voltage source converter (4LVSC), voltage control, grid-forming, full state feedback law, nonlinear unbalanced system.**

I. Introduction

THE development of future electrical power systems is focused on increasing energy efficiency, reducing the dependency of fossil fuels and obtaining a greater advantage of the distributed energy resources (DER). Under these fundamental pillars, the creation and interconnection of microgrids [1] has emerged as a driver to enhance country's energy independence, whilst avoiding the investments on large power transmission systems. Microgrids are characterized by an integration in the same distribution network of generation resources, storage and consumption of electrical energies operating in both connected to the main electrical system or isolated in emergency situations [2], [3]. The main difference between a traditional distribution network and a microgrid with DERs consists of the coordinated management of the different generation sources, storage and controllable loads [4]. In order to perform this task, it is essential that the local controller of each DER can have an adequate tracking of the references that are provided from a superior control layer, while guaranteeing a high quality power supply [5], [6]. Most DERs require an interface to be connected to microgrids. This function is usually developed by a voltage source converter (VSC) [7] that replaces the synchronous machine. Therefore, an appropriate control of the VSC will allow to integrate efficiently the DERs according to the requirements of the microgrids.

The deployment of the microgrids is intended to be at distribution level where the network is three-phase with neutral (four wires) in order to supply power not only to three-phase but also to single-phase loads. Hence, the topology of the VSC that interconnects the DERs to the microgrid has to be three-phase four wire. In the specific literature, several configurations of VSC have been proposed to obtain the fourth wire in power converters. A simple approach is based on maintain three-phase three wire power converter topology adding a Δyn transformer after the interconnection filter [8]. In this way, the fourth wire is connected to the network side of the transformer and not to the power converter. In order to avoid the transformer connection, a well-known structure is the topology called split DC-link. This method divides the DC bus by means of two capacitors connecting the fourth cable to the midpoint [9]. If this converter is connected to an unbalanced voltage, an uncontrolled 2ω voltage ripple appears on the DC bus. This could lead one capacitor to be more charged than its rated value, causing possible damage to the VSC components. An interesting proposal that increases the control capacity of the converter is the connection of an additional branch of semiconductors, known as four-leg VSC (4LVSC). This configuration allows to control the voltage in the neutral wire [10] reducing the overvoltage problems in the capacitors. Several applications to solve problems of line harmonic currents and neutral line currents [11] and reactive power compensation [12] of LV distribution system has been satisfactory proposed using this topology.

The performance of a converter depends on its controller, which in turn depends on its operation mode. In [13] three operation modes for power converters were highlighted: (i) grid-feeding, (ii) grid-supporting, and (iii) grid-forming.

The grid-feeding mode consists in delivering power to an energized grid. A synchronization stage and a current control loop are implemented in the local control of the VSC which allows to obtain the desired powers. Several current control algorithms in stationary and rotating frame have been

Manuscript received February 20, 2019; revised June 3, 2019 and September 18, 2019; accepted November 27, 2019.

This work was supported in part by Universidad de Sevilla in the framework of VI PPIT-US. This work is also part of EASY-RES project that has received funding from European Union's Horizon 2020 Research and Innovation programme under Grant Agreement No 764090.

The authors are with the Department of Electrical Engineering, Universidad de Sevilla, Seville 41092, Spain (e-mail: jolives@us.es; j.m.mauricio@ieee.org; manuelbarragan@us.es; fmatas@us.es).

presented in the literature to achieve the intended goal under balanced and unbalanced grid conditions [14]–[17].

The grid-supporting converters are divided into two control modes: current and voltage. The first case can be considered an evolution of grid-feeders power converters. Their power references are modified to contribute in regulating the grid voltage frequency and amplitude. Examples may include injection of reactive power for imbalance compensation by STATCOM [18]–[21]. The voltage control mode can be construed as an extension of grid-forming converter in order to connect it safely to the main grid. This kind of converters includes a voltage control loop to regulate the amplitude and frequency of the grid voltage. The most known example is the Virtual Synchronous Machine [22], [23]. Other algorithms are those focused on voltage regulation through droop [24], [25].

The grid-forming mode works as an ideal ac voltage source with a given amplitude and frequency. They may set the reference in an isolated grid and operate in parallel with other grid-forming converters or synchronous generators. This method is usually based on a cascaded controller composed of an outer voltage control loop and an inner current control loop. A control strategy on a rotating reference frame to feed unbalanced loads was presented in [26], [27] for 4LVSC. However, only linear loads and steady-state performance were considered. In [28] the work was extended to transient-state but again with linear loads only. The operation with nonlinear loads was presented in [29]. This is done in a stationary frame by adding resonant controllers tuned at the frequency of each harmonic to be compensated at the PCC into the voltage and current control loops. This approach requires to know the order of the harmonics absorbed by the loads to select the proper frequencies in the resonant controllers. If a new load is connected in the system absorbing current harmonics of a different order, the voltage at the PCC is distorted by this harmonic reducing its wave quality. Moreover, the addition of resonant controllers implies a high computational cost that could cause a malfunction of the microcontroller or reduce the number of harmonics to be compensated due to this issue.

This paper presents a novel approach of the voltage control of 4LVSC in stationary frames for grid-forming operation mode connected to the PCC through an LC-filter. The main objective of the controller is to provide a balanced three-phase voltage at the PCC under the presence of any type of generation or load: linear, nonlinear, balanced and unbalanced as well as a combination of these. The control algorithm is based on full state feedback law with a dynamic extension of the plant by adding resonant structures [30] tuned to the fundamental frequency and applied to the error of the voltages in order to assure zero steady-state error. To maintain the same number of sensors and I/O signals than those used in the classical controller structure, the measurements considered are the capacitors voltage and the currents injected into the PCC. The advantages that justify the use of these measurements are detailed below. Therefore, this decision leads to the states corresponding to the current through the inductors being unknown and to the impossibility of implementing the complete state feedback law. To deal with it, a Luenberger observer is proposed to estimate the states of the plant from the measurements considered and successfully execute the proposed control strategy. The controller gains are computed by formulating a linear quadratic regulator (LQR) problem applied to the extended model. The main advantages of this method are that it guarantees small signal stability, its design is independent of the type of load connected into the PCC and it provides active damping to the system avoiding using additional resistors that would reduce the performance of the 4LVSC integration.

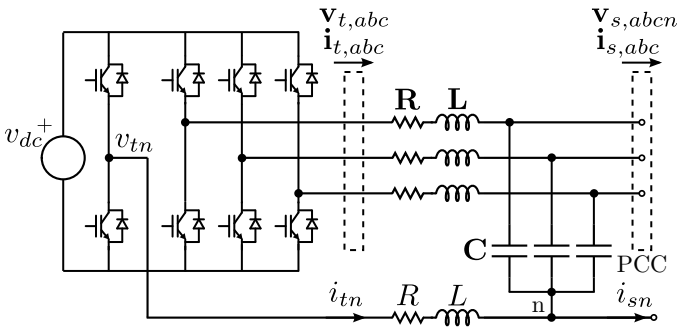

Fig. 1. Four-Leg Voltage Source Converter connected to a PCC through an LC-filter.

The main contributions of the paper include: 1) novel approach for controlling the voltage of the 4LVSC under grid-forming operation mode based on full state feedback law; 2) developing a systematic methodology for tuning the controller gains ensuring stability, robustness and offering active damping; 3) experimental validation of the proposed controller obtaining high quality voltages.

The rest of the paper is organized as follows. Section II presents the mathematical description of a 4LVSC connected to the network through an LC-filter. In Section III, the design of the voltage control algorithm is developed from the mathematical model. Section IV depicts and discusses the performance of the proposed control strategy via experimental results in different test cases for steady- and transient-state. The paper closes with the main conclusions.

II. Mathematical Description of the Four-Leg VSC

In this section, the mathematical model of the 4LVSC in the *abc* reference frame is presented. Then, this model is transformed to $\alpha\beta\gamma$ framework.

Fig. 1 shows a 4LVSC connected to a PCC through an LC-filter. Note that a filter inductor is also connected to the neutral wire to mitigate the high frequency harmonics of the IGBTs switching. The DC-side of the power converter is considered to be connected to an infinite power DC voltage source. Consequently, the dynamics from the DC voltage is omitted for the model development.

The differential-algebraic set of equations that models the

dynamics of the system in *abc* frame can be written as:

$$\mathbf{v}_{t,abc} - v_{tn} = \mathbf{R}\mathbf{i}_{t,abc} + \mathbf{L}\frac{d\mathbf{i}_{t,abc}}{dt} + \mathbf{v}_{s,abcn} - \Delta v_{tn}, \quad (1a)$$

$$\Delta v_{tn} = Ri_{tn} + L\frac{di_{tn}}{dt}, \quad (1b)$$

$$\mathbf{i}_{t,abc} - \mathbf{i}_{s,abc} = \mathbf{C}\frac{d\mathbf{v}_{s,abcn}}{dt}, \quad (1c)$$

$$0 = i_{sa} + i_{sb} + i_{sc} + i_{sn}, \quad (1d)$$

where $\mathbf{v}_{s,abc} = [v_{sa}\ v_{sb}\ v_{sc}]^T$ indicates the voltage across the capacitors which is measured against n point, $\mathbf{v}_{t,abc} = [v_{ta}\ v_{tb}\ v_{tc}]^T$ is the 4LVSC terminal voltage, $\mathbf{i}_{t,abc} = [i_{ta}\ i_{tb}\ i_{tc}]^T$ is the current circulating through the filter inductor and $\mathbf{i}_{s,abc} = [i_{sa}\ i_{sb}\ i_{sc}]^T$ represents the current injected into the PCC. The filter inductance, resistance and capacitance are represented by matrices $\mathbf{L} = diag\,[L\ L\ L]$, $\mathbf{R} = diag\,[R\ R\ R]$ and $\mathbf{C} = diag\,[C\ C\ C]$, respectively. Equation (1d) defines the Kirchhoff's currents law constraint at the PCC.

The set of dynamic equations (1) can be transformed into the stationary reference frame $\alpha\beta\gamma$ by using the Clarke transformation. In this way, these equations can be expressed in the new coordinates $\alpha\beta\gamma$ as follows:

$$\mathbf{v}_{t,\alpha\beta\gamma} = \mathbf{R}\mathbf{i}_{t,\alpha\beta\gamma} + \mathbf{L}\frac{d\mathbf{i}_{t,\alpha\beta\gamma}}{dt} + \mathbf{v}_{s,\alpha\beta\gamma}, \quad (2a)$$

$$\mathbf{i}_{t,\alpha\beta\gamma} - \mathbf{i}_{s,\alpha\beta\gamma} = \mathbf{C}\frac{d\mathbf{v}_{s,\alpha\beta\gamma}}{dt}, \quad (2b)$$

where the matrices of the system parameters are updated as: $\mathbf{R} = diag\,[R\ R\ 4R]$, $\mathbf{L} = diag\,[L\ L\ 4L]$, and $\mathbf{C} = diag\,[C\ C\ C]$, and the vectors of the variables are expressed in $\alpha\beta\gamma$ frame. Note that (1d) is an intrinsic part of this set of equations due to $i_{sn} = i_{s\gamma}/\sqrt{3}$.

III. Voltage Control Algorithm Design

In this section, a control strategy consisting of full state feedback law is designed on $\alpha\beta\gamma$ frame to regulate the voltages at the PCC. The main objective is to maintain a pure sinusoidal and balanced three-phase voltage in presence of linear and nonlinear loads with any degree of imbalance.

The proper development of the proposed control strategy requires knowing both the states of the plant, i.e., the capacitor voltage $\mathbf{v}_{s,\alpha\beta\gamma}$ and the inductor current $\mathbf{i}_{t,\alpha\beta\gamma}$, and the internal states of the controller defined in Section III-B. The classical approaches to obtain the states of the plant measure them directly without taking into account the current $\mathbf{i}_{s,\alpha\beta\gamma}$ injected to the PCC. This current, in spite of not being a state of the plant, provides several advantages with respect to $\mathbf{i}_{t,\alpha\beta\gamma}$ as: i) the harmonic distortion due to switching frequency is lower obtaining a less polluted waveform in the signals used by the controller, and, ii) during transient phenomena, the current supplied by the capacitors discharge is reflected in $\mathbf{i}_{s,\alpha\beta\gamma}$ allowing the controller to act faster and protect the VSC. For these reasons, this paper proposes to measure $\mathbf{v}_{s,\alpha\beta\gamma}$ and $\mathbf{i}_{s,\alpha\beta\gamma}$ to implement the control strategy. Note that number of measurements of this proposal is identical to the classical controller without adding extra cost to the device.

This choice leads to the fact that the state subset of the plant $\mathbf{i}_{t,\alpha\beta\gamma}$ must be computed from the previous measurements. In this way, it is proposed a control algorithm based on two stages as shown in Fig. 2. The first stage of the controller is a Luenberger observer which estimates the states of the plant from the measurements. The second stage is the voltage control loop based on full state feedback which receives the estimated states and computes the voltage at VSC terminals, $\mathbf{v}_{t,\alpha\beta\gamma}$. This stage is designed extending the plant dynamic by adding a resonant structure to the voltage error of each $\alpha\beta\gamma$ component. In this way, it can be considered that this strategy is composed of a single control loop inherent to full state feedback law, unlike the classical cascade control for grid-forming operation mode [13] which contains an outer voltage control loop and inner current control loop.

The following subsections detail the two stages of the control algorithm, the computation of controller gains and a voltage droop method to protect the VSC in case of overcurrents.

A. First Stage: State Observer

The purpose of this stage is to estimate the voltages across the capacitors and the currents through the inductors, which are the state variables of the plant, from the available measurements detailed above.

A state observer is defined in [31] as a subsystem to reconstruct the state vector of a plant. Therefore, its mathematical model is fundamentally the same as that of the plant. The only difference is that an additional term is included to weight the estimation error. This term compensates for the inaccuracies of the model as well as the lack of knowledge of the initial state error.

Let the plant dynamics given by (2) be expressed in a compact form as:

$$\dot{\mathbf{x}}_p = \mathbf{A}_p\,\mathbf{x}_p + \mathbf{B}_p\,\mathbf{u}_p, \quad (3a)$$

$$\mathbf{y}_p = \mathbf{C}_p\,\mathbf{x}_p, \quad (3b)$$

where the subscript p is used to indicate *plant*, $\mathbf{x}_p = [\mathbf{v}_{s,\alpha\beta\gamma}\ \mathbf{i}_{t,\alpha\beta\gamma}]$ represents the state variables, $\mathbf{y}_p = \mathbf{v}_{s,\alpha\beta\gamma}$ is the system output vector and the vector of system inputs $\mathbf{u}_p = [\mathbf{v}_{t,\alpha\beta\gamma}\ \mathbf{i}_{s,\alpha\beta\gamma}]$ is the voltage at the terminals of the VSC and the current injected to the PCC.

By applying the Luenberger state observer definition [32] over (3), the following system is obtained:

$$\dot{\tilde{\mathbf{x}}}_p = \mathbf{A}_p\,\tilde{\mathbf{x}}_p + \mathbf{B}_p\,\mathbf{u}_p + \mathbf{G}\,(\mathbf{y}_p - \tilde{\mathbf{y}}_p), \quad (4a)$$

$$\tilde{\mathbf{y}}_p = \mathbf{C}_p\,\tilde{\mathbf{x}}_p, \quad (4b)$$

where $\tilde{\mathbf{x}}_p$ is the estimated vector state, $\tilde{\mathbf{y}}_p$ is the estimated output, $(\mathbf{y}_p - \tilde{\mathbf{y}}_p)$ is the estimation error, and $\mathbf{G}$ is the additional term called weighting matrix. The values of $\mathbf{G}$ define the performance of the observer and they are computed by solving an LQR problem using (3) as a constriction. In this way, it is ensured that the estimation error converges to zero. The LQR problem is solved by using the Matlab function `lqrd.m`.

From the input $\mathbf{u}_p$ and the output $\mathbf{y}_p$, the estimated state vector $\tilde{\mathbf{x}}_p$ can be computed by using (4) obtaining the current through the inductors, $\tilde{\mathbf{i}}_{t,\alpha\beta\gamma}$. Furthermore, the observer

estimates the voltages across the capacitors, $\tilde{\mathbf{v}}_{s,\alpha\beta\gamma}$, which is equivalent to filter the measurement of $\mathbf{v}_{s,\alpha\beta\gamma}$. The use of $\tilde{\mathbf{v}}_{s,\alpha\beta\gamma}$ instead of $\mathbf{v}_{s,\alpha\beta\gamma}$ in the controller improves the performance of the whole algorithm.

B. Second Stage: Voltage Control Loop

The aim of this stage is to determine proper voltages at the terminals of the VSC to establish the desired voltages at the PCC. To achieve this, a control law based on the full state feedback theory is formulated in $\alpha\beta\gamma$ frame.

The system input subset, $\mathbf{u}'_p = \mathbf{v}_{t,\alpha\beta\gamma}$, is obtained applying the state feedback law over the model of the plant (3) as:

$$\mathbf{u}'_p = \mathbf{K}_f\, \boldsymbol{\varepsilon}_p, \tag{5}$$

where $\mathbf{K}_f = [\mathbf{K}_i\ \mathbf{K}_v]$ contains the feedback gains and $\boldsymbol{\varepsilon}_p = [\boldsymbol{\varepsilon}_i\ \boldsymbol{\varepsilon}_v]^T$ represents the set of state errors. These are defined as:

$$\boldsymbol{\varepsilon}_i := \mathbf{i}^\star_{t,\alpha\beta\gamma} - \tilde{\mathbf{i}}_{t,\alpha\beta\gamma}, \tag{6a}$$

$$\boldsymbol{\varepsilon}_v := \mathbf{v}^\star_{s,\alpha\beta\gamma} - \tilde{\mathbf{v}}_{s,\alpha\beta\gamma}, \tag{6b}$$

where $\tilde{\mathbf{i}}_{t,\alpha\beta\gamma}$ and $\tilde{\mathbf{v}}_{s,\alpha\beta\gamma}$ are the estimated states obtained as explained in Section III-A and the references $\mathbf{v}^\star_{s,\alpha\beta\gamma}$ and $\mathbf{i}^\star_{t,\alpha\beta\gamma}$ are detailed below.

The desired voltages set at the PCC, $\mathbf{v}^\star_{s,\alpha\beta\gamma}$, is a sinusoidal balanced symmetrical three-phase voltage. These references, which are characterized by a constant magnitude, V, frequency, ω, and phase, ϕ, are expressed on the stationary frame as:

$$\mathbf{v}^\star_{s,\alpha\beta\gamma} = V \begin{bmatrix} \sin(\omega t + \phi) & -\cos(\omega t + \phi) & 0 \end{bmatrix}^T. \tag{7}$$

The current references set $\mathbf{i}^\star_{t,\alpha\beta\gamma}$ can not be imposed *a priori* since it depends on the connected load. However, it is necessary that every signal that feeds the controller converges to zero. Thus, $\mathbf{i}_{s,\alpha\beta\gamma}$ is used in a feedforward loop as the current references set, $\mathbf{i}^\star_{t,\alpha\beta\gamma}$. On the one hand, this approach assumes a marginal error at steady state because both currents are not equal but practically identical for low order harmonics as the fundamental frequency. Note that within this frequency range the capacitors present high impedance. On the other hand, this decision allows to anticipate fault currents, as explained in Section III-D.

It is worth stressing that the voltage references are sinusoidal signals and, consequently, the state feedback (5) does not guarantee a zero steady-state error for $\mathbf{v}_{s,\alpha\beta\gamma}$. It becomes necessary to include an oscillating structure, also known as resonant structure, in order to achieve a proper tracking, as it is stated in the internal model principle of control theory [33].

The differential equations that model the oscillator dynamics can be written as follows:

$$\dot{\mathbf{r}} = \omega' \left(\boldsymbol{\nu} - \mathbf{q}\right), \tag{8a}$$

$$\dot{\mathbf{q}} = \omega'\, \mathbf{r}, \tag{8b}$$

where ω' is the oscillation frequency, $\boldsymbol{\nu}$ is the oscillator input vector, and $\mathbf{r}$ and $\mathbf{q}$ are the in-quadrature dynamic states defined in $\alpha\beta\gamma$ frame. Note that (8) is the well-known second order generalized integrator (SOGI) [30]. This scheme can be written in a state-space form as:

$$\dot{\mathbf{x}}_o = \mathbf{A}_o\, \mathbf{x}_o + \mathbf{B}_o\, \mathbf{u}_o, \tag{9}$$

where:

$$\mathbf{A}_o = \begin{bmatrix} \mathbf{0} & -\mathbf{W} \\ \mathbf{W} & \mathbf{0} \end{bmatrix}, \mathbf{B}_o = \begin{bmatrix} \mathbf{0} & \mathbf{W} \\ \mathbf{0} & \mathbf{0} \end{bmatrix},$$
$$\mathbf{W} = diag \begin{bmatrix} \omega' & \omega' & \omega' \end{bmatrix}.$$

Setting $\omega = \omega'$, $\mathbf{u}_o = \boldsymbol{\varepsilon}_p$ and $\mathbf{x}_o = [\mathbf{r}\ \mathbf{q}]^T$ allows to build an extended model combining SOGI (8) and plant dynamics (3). The state-space of the open loop extended model is as follows:

$$\begin{bmatrix} \dot{\mathbf{x}}_p \\ \dot{\mathbf{x}}_o \end{bmatrix} = \begin{bmatrix} \mathbf{A}_p & \mathbf{0} \\ \mathbf{B}_o & \mathbf{A}_o \end{bmatrix} \begin{bmatrix} \mathbf{x}_p \\ \mathbf{x}_o \end{bmatrix} + \begin{bmatrix} \mathbf{B}_p \\ \mathbf{0} \end{bmatrix} \mathbf{u}_p. \tag{10}$$

In order to close the loop, the full state feedback law is applied to the above extended state space obtaining:

$$\mathbf{u}'_p = \mathbf{K}_i \boldsymbol{\varepsilon}_i + \mathbf{K}_v \boldsymbol{\varepsilon}_v + \mathbf{K}_r \mathbf{r} + \mathbf{K}_q \mathbf{q}, \tag{11}$$

where $\mathbf{u}'_p = \mathbf{v}_{t,\alpha\beta\gamma}$ is the voltage set which guarantees a zero tracking error for the desired voltage at the PCC.

Equations (9) and (11) define the model of the voltage control loop as depicted in Fig. 2.

C. Control Gains Tuning

This section is focused on explaining the systematic process used to calculate the controller gains. The approach was to solve an LQR problem [31] constrained by the extended dynamic model (10). The weighting matrices of the LQR problem, $\mathbf{Q}$ and $\mathbf{R}$, establish the relative importance of the error and the energy involved during the transient response.

Considering that both matrices are of the adequate size, they must fulfill the following numerical constraints:

- $\mathbf{Q} = \mathbf{Q}^T$ and positive semi-definite.
- $\mathbf{R} = \mathbf{R}^T$ and positive definite.

Several iterations are generally required in a trial and error process for the selection of the weighting matrices. Taking into account Bryson's method [34] and considering that the ratio between the extended state vector and $\mathbf{u}'_p$ is one, it can be concluded that the identity matrix for both $\mathbf{Q}$ and $\mathbf{R}$ is a good starting point to initialize these matrices. The gains resulting from the LQR problem solved with these weighting matrices are evaluated by simulation. The response of the controller is analyzed in terms of the settling time and overshoot and, thus, the values of $\mathbf{Q}$ and $\mathbf{R}$ are modified to improve the controller output. The objective is to keep the settling time less than one cycle of the voltage wave, and avoid overshoot, which in the system would result in overvoltage.

Control gains tuned by solving an LQR problem subject to the extended state-space guarantees small signal stability offering a high degree of robustness against unknown load conditions. Moreover, including the dynamics of the plant also provides active damping to the system. Therefore, the power converter performance improves by reducing the power losses because no additional resistors have to be connected.

This article has been accepted for publication in a future issue of this journal, but has not been fully edited. Content may change prior to final publication. Citation information: DOI 10.1109/TEC.2019.2957185, IEEE Transactions on Energy Conversion

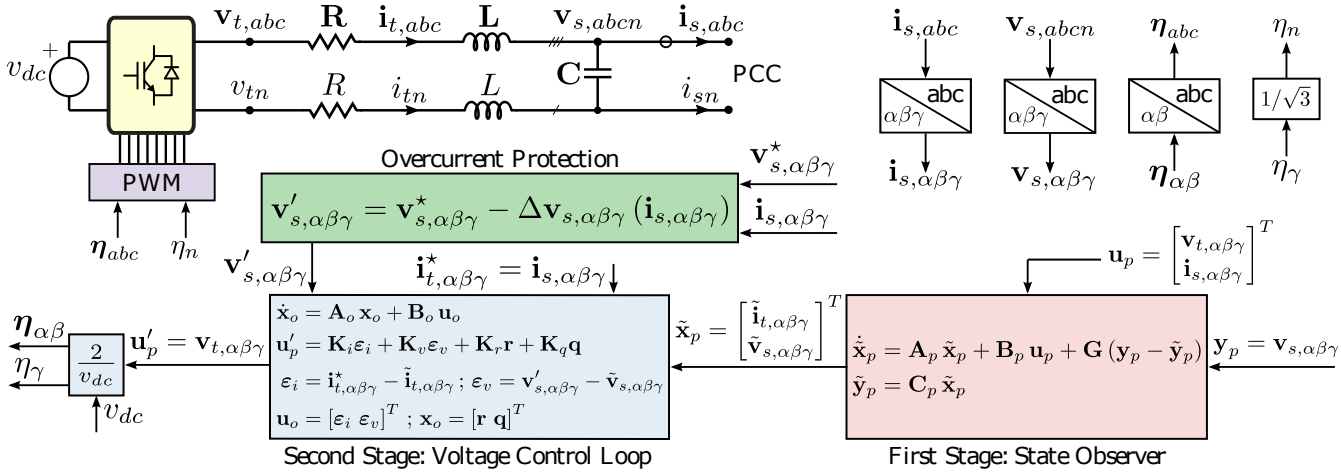

Fig. 2. Proposed voltage control algorithm.

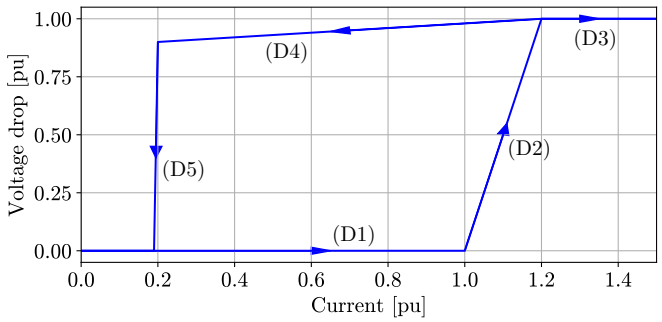

Fig. 3. Voltage drop droop characteristics as a function of current.

D. Overcurrent Protection

The proposed control strategy operates the VSC as a grid-forming power converter establishing the voltage at the PCC and supplying the necessary current demanded by the load. Under normal operation conditions, i.e., currents lower than the VSC rated current, the device can be considered as an ideal voltage source with a given magnitude and frequency. However, the converter must also be able to operate under overcurrent situations, as faults, avoiding to damage the device components. The adopted approach to deal with overcurrent operations is to define the amplitude of the voltage reference as a function of the injected current. The information regarding the measurement of the current $\mathbf{i}_{s,\alpha\beta\gamma}$ becomes relevant because the response of the capacitors is reflected in this current allowing to anticipate load variations. Therefore, when the current injected to the PCC is greater than the rated current, a voltage drop is added to the voltage reference as follows:

$$\mathbf{v}'_{s,\alpha\beta\gamma} = \mathbf{v}^{\star}_{s,\alpha\beta\gamma} - \Delta\mathbf{v}_{s,\alpha\beta\gamma}\left(\mathbf{i}_{s,\alpha\beta\gamma}\right), \tag{12}$$

where $\Delta\mathbf{v}_{s,\alpha\beta\gamma}\left(\mathbf{i}_{s,\alpha\beta\gamma}\right)$ is obtained from the droop characteristic depicted in Fig. 3. Note that (6) must be updated with the voltage reference computed in (12) as shown in Fig. 2.

From Fig. 3 it can be seen that during the operation under rated currents (D1) no voltage drop is applied to the reference $\mathbf{v}^{\star}_{s,\alpha\beta\gamma}$. When $\mathbf{i}_{s,\alpha\beta\gamma}$ exceeds the rated value, a proportional voltage drop (D2) is applied on the reference to reduce the contribution of the power converter. If $\mathbf{i}_{s,\alpha\beta\gamma}$ differs significantly from its rated value ($\mathbf{i}_{s,\alpha\beta\gamma} \geq 1.20$ pu), the voltage drop is blocked at 1 pu (D3). In order to detect if the fault is cleared a soft ramp (D4) reduces the voltage drop. While the current remains high, the voltage drop continues being applied. This situation is maintained until the current is less than a security value (0.2 pu) when the voltage drop is completely removed (D5).

The behaviour of this proposed overcurrent protection was validated via hardware in the loop (HIL) simulation using the Typhoon HIL 402-01-005 platform. The results will be presented in Section IV-D.

E. Modulation Stage

The modulation stage is responsible for transforming the outputs of the controller to the gate signals to switch the IGBTs. Firstly, the control output signals are scaled to compute the modulation signals as follows:

$$\boldsymbol{\eta}_{\alpha\beta\gamma} = \frac{2}{v_{dc}}\mathbf{v}_{t,\alpha\beta\gamma}. \tag{13}$$

Modulation signals in $\alpha\beta\gamma$ frame must be transformed to the natural frame abc in order to operate the IGBTs. In this case, the structure of the four-leg VSC increases the complexity of this task due to the fourth signal required to control the fourth leg. To accomplish it, the approach used is based on splitting the information of the symmetric vectors, i.e. positive and negative sequence, from that of the zero component. Therefore, $\boldsymbol{\eta}_{abc}$ is computed from $\boldsymbol{\eta}_{\alpha\beta}$ by means of the simplified Clarke inverse transformation. This is equivalent to operate a three-phase VSC with insulated neutral. Whereas η_n is determined by resizing γ component as: $\eta_n = \eta_\gamma/\sqrt{3}$ compensating the zero sequence. This simplification, shown in Fig. 2, allows a significant reduction on the computational burden with respect to the three-dimensional space vector modulation presented in [35].

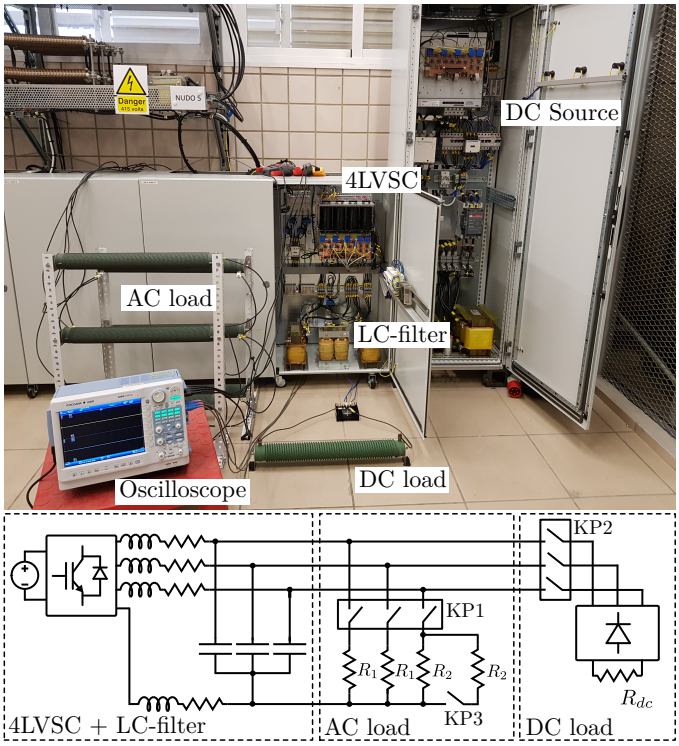

Fig. 4. (a) Laboratory experimental test bench. (b) Block diagram.

IV. Experimental Results

The effectiveness of the proposed control algorithm is validated experimentally by using a 4LVSC connected to several loads through an LC-filter. The experimental setup assembled to develop the test in the laboratory environment is presented in Fig. 4. Most relevant parameters of the system are collected in Table I. This setup consists of two VSCs with back-to-back topology that share a common DC bus. VSC1 is a three-phase three wire device whose AC side is connected to the low voltage laboratory network and it is in charge to control the DC voltage level of the common DC bus. In this way, this power converter acts as the DC voltage source presented in Fig. 1. VSC2 is the 4LVSC responsible of establishing the voltage at the PCC according to the controller presented in Section III. The parameters of the controller are determined considering the data of Table I as,

$$\mathbf{G} = \begin{bmatrix} -5.4 & 0 & 0 & -20.3 & 0 & 0 \\ 0 & -5.4 & 0 & 0 & -20.3 & 0 \\ 0 & 0 & -1.2 & 0 & 0 & 23.9 \end{bmatrix}^T 10^{-3},$$

$$\mathbf{K}_i = \begin{bmatrix} 30.20 & 30.20 & 74.670 \end{bmatrix},$$
$$\mathbf{K}_v = \begin{bmatrix} -0.09 & -0.09 & 0.12 \end{bmatrix},$$
$$\mathbf{K}_r = \begin{bmatrix} 1.0 & 1.0 & 1.22 \end{bmatrix},$$
$$\mathbf{K}_q = \begin{bmatrix} 0.24 & 0.24 & 0.28 \end{bmatrix}.$$

Matrices $\mathbf{A}_p$, $\mathbf{B}_p$, $\mathbf{C}_p$, $\mathbf{A}_o$, and $\mathbf{B}_o$ in turn are easily obtained from Sections III-A and III-B. The control algorithm was implemented in a TMS320F28335 Delfino microcontroller from Texas Instruments setting a sampling frequency of 20 kHz. The loads are connected to the 4LVSC through the operation of several breakers. This make it possible that different types of loads can be easily connected and disconnected during the operation of the 4LVSC. The following experimental tests can be executed:

- *Test 1*. Three-phase resistive balanced and linear load of 50 Ω per phase. KP1: ON, KP2: OFF and KP3: ON.
- *Test 2*. An additional nonlinear load composed of a diode bridge rectifier and a 100 Ω resistor is added to the previous test. KP1: ON, KP2: ON and KP3: ON.
- *Test 3*. From the *Test 2*, the balanced load is unbalanced increasing the resistance of phase *a* to 100 Ω. KP1: ON, KP2: ON and KP3: OFF.
- *Test 4*. Only the nonlinear load is connected. KP1: OFF, KP2: ON and KP3: OFF.

TABLE I
Parameters of the Experimental Setup

Parameter	Value
v_{dc} DC bus voltage	730 V
RMS AC rated voltage of 4LVSC	400 V
RMS AC rated current of 4LVSC	40 A
Switching frequency	10 kHz
Sampling frequency of DSP	20 kHz
L Filter inductance	5 mH
R Filter resistance	0.1 Ω
C Filter capacitance	1 μF
R_1 AC load	50 Ω
R_2 AC load	100 Ω
R_{dc} DC load	100 Ω

The performance of the controller is evaluated in steady- and transient-state for each test and transition. Moreover, a comparison between the classical [13] and the proposed controller is made for *Test 1* and *Test 4* in order to evaluate both strategies under different type of loads. For this purpose, the total harmonic distortion (THD) of voltages, THD_v, and currents, THD_i, as well as the relationship between the negative and positive sequence of the measured current, (I_s^-/I_s^+), and voltage, (V_s^-/V_s^+), are analyzed according to the UNE-EN 50160 standard. This standard establishes a maximum imbalance, V_s^-/V_s^+, equal to 2.0 % for the electricity supplied by public distribution systems. In addition, the maximum THD_v is limited up to 8.0 %, calculated up to the 40^{th} harmonic.

Finally, the controller is tested for a three-phase fault at the PCC in order to evaluate the effectiveness of the overcurrent protection. This test was performed via HIL using the Typhoon HIL 402-01-005 platform. Therefore, the control algorithm can be safely tested in the microcontroller without jeopardizing the power converter.

A. Steady-state performance

Table II shows the experimental results obtained in steady-state for each test with the proposed controller when the set-point of the voltages at the PCC is established to 230 V/phase (RMS value) and a fundamental frequency of 50 Hz.

The results of *Test 1* show that the THD_v is practically zero indicating that the voltage at the PCC is a 50 Hz sine

TABLE II
STEADY-STATE EXPERIMENTAL RESULTS OF THE TESTS USING THE PROPOSED VOLTAGE CONTROL ALGORITHM.

Test	THD_v	THD_i	V_s^-/V_s^+	I_s^-/I_s^+
Test 1	0.2 %	0.5 %	0.3 %	0.3 %
Test 2	3.18 %	17.19 %	0.33 %	0.52 %
Test 3	3.22 %	18.47 %	0.39 %	9.93 %
Test 4	3.24 %	36.28 %	0.29 %	0.72 %

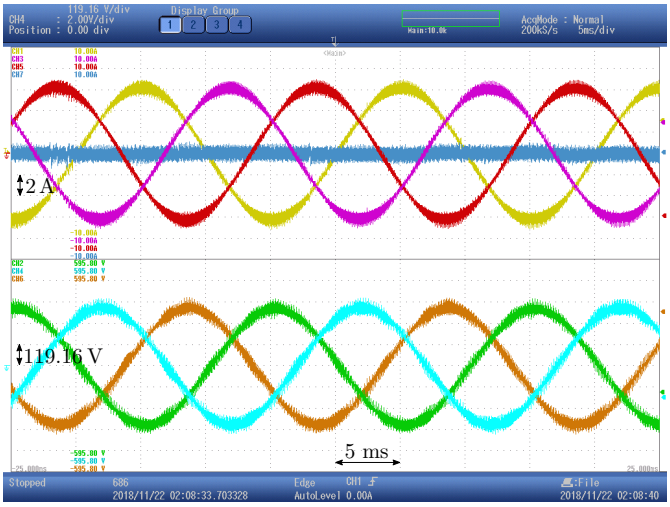

Fig. 5. Steady-state of *Test 1*. Top: $i_{s,a}$ (yellow), $i_{s,b}$ (purple), $i_{s,c}$ (red) and $i_{s,n}$ (blue). Bottom: $v_{s,an}$ (green), $v_{s,bn}$ (light blue) and $v_{s,cn}$ (orange).

wave. The THD_i yields similar results to the THD_v due to the current flowing to the load is proportional to the voltage at the PCC for linear loads. Moreover, the imbalance indexes present a low value for voltages and currents which means that the voltages generated at the PCC have a very high degree of balance. These effects can be also observed in Fig. 5 where the three-phase currents and voltages are depicted using a Yokogawa DL850 oscilloscope during the test. The set of signals observed in the top plot of the screenshot corresponds to the currents flowing towards the load. The yellow, purple and red curves represent the currents i_{sa}, i_{sb} and i_{sc} respectively and the blue curve shows the current of the neutral wire, i_{sn}. The set of signals of the bottom plot reflects the voltage measured at terminals of the capacitors where the PCC is located. The green, light blue and orange curves show the voltages v_{san}, v_{sbn} and v_{scn} respectively. The waveform of the voltages is sinusoidal at a frequency of 50 Hz and a RMS value of 230 V according to the references given to the controller. The bands superimposed on the sine waves correspond to the harmonics of high frequency due to the switching of the IGBTs. These have a reduced impact on the performance of the electrical systems because they barely affect to the loads, generators and electrical lines of the network.

In *Test 2*, the nonlinear load is added to the balanced linear load producing a high distortion in the current as reflected in a large THD_i value. The results show that the THD_v worsens with respect to *Test 1* due to the distortion caused by the

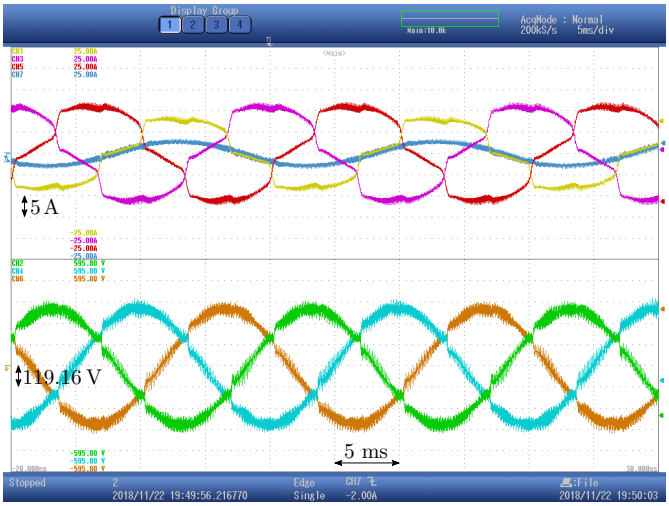

Fig. 6. Steady-state of *Test 3*. Top: $i_{s,a}$ (yellow), $i_{s,b}$ (purple), $i_{s,c}$ (red) and $i_{s,n}$ (blue). Bottom: $v_{s,an}$ (green), $v_{s,bn}$ (light blue) and $v_{s,cn}$ (orange).

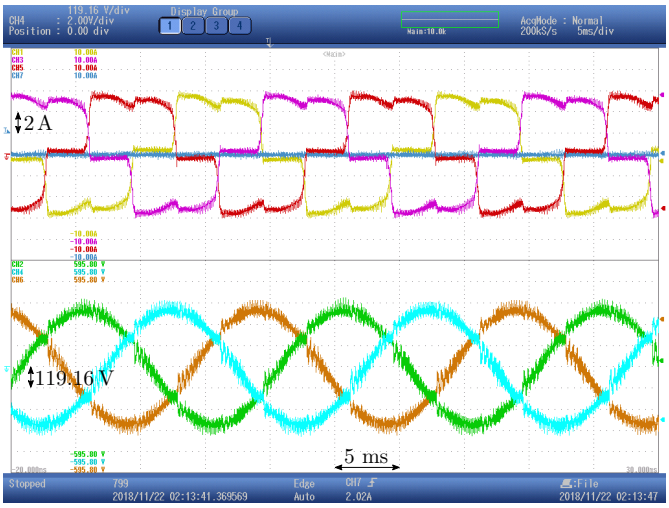

Fig. 7. Steady-state of *Test 4*. Top: $i_{s,a}$ (yellow), $i_{s,b}$ (purple), $i_{s,c}$ (red) and $i_{s,n}$ (blue). Bottom: $v_{s,an}$ (green), $v_{s,bn}$ (light blue) and $v_{s,cn}$ (orange).

nonlinear load. Despite this increase, this value continues to be within the limits established by the UNE-EN 50160 standard with a wide margin. The degree of imbalance of the voltage and current is maintained at a reduced value indicating that the nonlinear load has a minimum influence in the negative sequence.

In *Test 3*, the linear load is unbalanced by increasing the resistance of phase a from 50 to 100 Ω. This effect can be observed at the top plot of Fig. 6 where the amplitude of the yellow current is lower than the other two phase currents causing a current circulation through the neutral wire. The THD_v and THD_i values are similar to the previous test because the nonlinear load is still present in the system. Despite the high degree of imbalance reflected in a large value of I_s^-/I_s^+, the imbalance index of the voltage is only $0.39\,\%$. It can be noted that the proposed voltage control maintains the voltages balanced in presence of unbalanced currents as shown in the bottom plot of Fig. 6.

TABLE III
STEADY-STATE EXPERIMENTAL RESULTS OF THE TESTS USING THE CASCADE CONTROL ALGORITHM.

Test	THD_v	THD_i	V_s^-/V_s^+	I_s^-/I_s^+
Test 1	0.72 %	0.67 %	0.69 %	0.69 %
Test 4	8.66 %	27.01 %	1.5 %	1.2 %

The results obtained from *Test 4* are depicted in Fig. 7. In this case, the currents are completely polluted by harmonics of order $6k \pm 1$ as shown in the top plot of Fig. 7 and the highest value of $THD_i = 36.28\,\%$. Nevertheless, the voltages maintain a good signal quality, $THD_v = 3.24\,\%$ similar to *Test 2* and *Test 3*, obtaining a sine wave of 50 Hz and 230 V RMS as shown in the bottom plot of Fig. 7.

B. Controllers comparison

This subsection is devoted to compare the performance of the voltage control algorithm presented in this work with respect to the classical cascade control. Table III collects the values of THD and imbalance of *Test 1* and *Test 4* for the cascade control. In *Test 1*, the value of all the indexes is around 0.7% indicating that both the harmonic distortion as the degree of imbalance are practically nonexistent in currents and voltages. This effect can be also observed in Fig. 8 where currents and voltages are almost pure sine waves of 50 Hz. The value of the indexes and the evolution of the measurements are very similar for both strategies under *Test 1*, see Table II and Fig. 5. Therefore, it can be affirmed that both controllers are capable of generating 50 Hz and 230 V RMS sinusoidal voltages at the PCC for linear loads.

The indexes of *Test 4* show very different results of THD between the cascade control and the proposed algorithm. Especially significant is the worsening of THD_v in the cascade control exceeding the maximum limit (8%) allowed by the UNE-EN 50160 standard. This distortion of the voltage waves is also reflected in Fig. 9 which cease to be purely sine waves. The voltage spectrum of both controllers and the limit values of the UNE-EN 50160 standard for most relevant harmonics are depicted in Fig. 10. It can be observed that no individual harmonic is exceeded with the proposed controller. However, the individual harmonics limits with the cascade control are violated from 11^{th} which leads a deterioration in the wave quality. One solution to improve the performance of the cascade controller with nonlinear loads is to add resonant controllers tuned to each harmonic order in parallel with the fundamental one. However, this approach increases the computational cost in the microcontroller and requires prior knowledge of the harmonic order absorbed by the load to properly adjust the resonant controllers.

C. Transient-state performance

This subsection presents the transient response of the proposed controller when the load varies abruptly by means of the breakers operation. Fig 11 shows the transient response produced when the 4LVSC is feeding the linear load and the

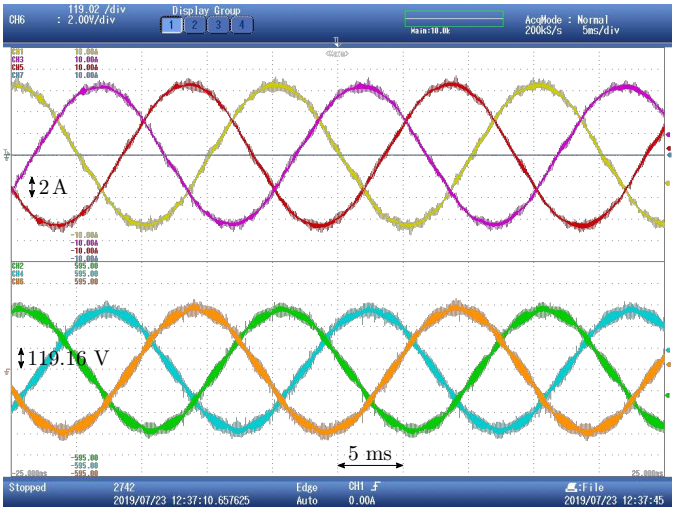

Fig. 8. Steady-state of *Test 1* for classical control. Top: $i_{s,a}$ (yellow), $i_{s,b}$ (purple), $i_{s,c}$ (red) and $i_{s,n}$ (blue). Bottom: $v_{s,an}$ (green), $v_{s,bn}$ (light blue) and $v_{s,cn}$ (orange).

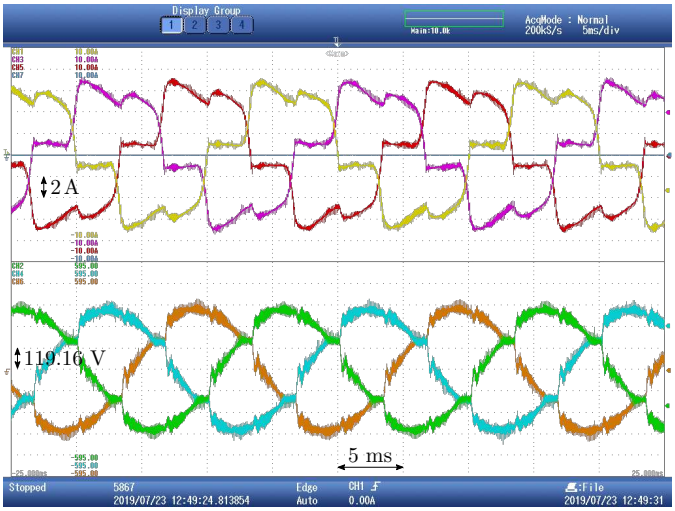

Fig. 9. Steady-state of *Test 4* for classical control. Top: $i_{s,a}$ (yellow), $i_{s,b}$ (purple), $i_{s,c}$ (red) and $i_{s,n}$ (blue). Bottom: $v_{s,an}$ (green), $v_{s,bn}$ (light blue) and $v_{s,cn}$ (orange).

nonlinear load is suddenly connected. It is observed how the purely sinusoidal balanced three-phase current is distorted by the harmonic content when the switch is closed. However, the voltages are barely perturbed and the sinusoidal waveform is maintained from one test to another. The only observable effect is a disturbance at the time of the change which is rapidly corrected by the controller. The time response of the control is less than 1 ms which represents the 5% of the fundamental period of the sine wave. Therefore, this disturbance has an inappreciable impact on the performance of the system.

Fig. 12 presents the three-phase current and voltage during the transition from *Test 3* to *Test 4*. Prior to the change, the currents are unbalanced and they are polluted by the harmonic content of the nonlinear load. The disconnection of the unbalanced linear loads leads the three-phase system to be balanced but completely nonlinear. In spite of this abrupt variation, the time response of the controller is about 1 ms

This article has been accepted for publication in a future issue of this journal, but has not been fully edited. Content may change prior to final publication. Citation information: DOI 10.1109/TEC.2019.2957185, IEEE Transactions on Energy Conversion

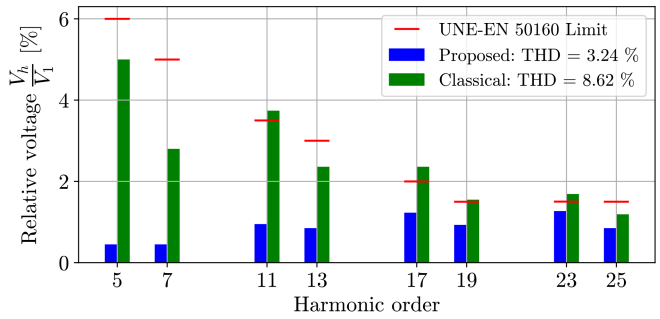

Fig. 10. *Test 4* voltage spectrum analysis for proposed (blue) and classical (green) controllers.

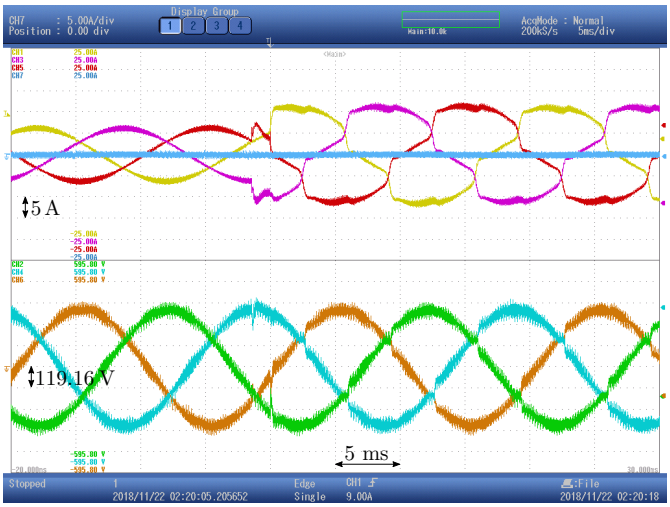

Fig. 11. Transient-state from *Test 1* to *Test 2*. Top: $i_{s,a}$ (yellow), $i_{s,b}$ (purple), $i_{s,c}$ (red) and $i_{s,n}$ (blue). Bottom: $v_{s,an}$ (green), $v_{s,bn}$ (light blue) and $v_{s,cn}$ (orange).

restoring the three-phase balanced voltage.

D. Three-phase fault

The overcurrent protection presented in Section III-D is evaluated via HIL simulation through a three-phase fault applied at the PCC. In this way, the algorithm can be executed in the microcontroller while the fault is being tested safely in the simulated 4LVSC.

Fig. 13 depicts the magnitudes $\mathbf{i}_{t,abc}$, $\mathbf{i}_{s,abc}$ and $\mathbf{v}_{s,abc}$ before, during and after the fault. This occurs at the time instant 0.04 s and it remains until the instant of time 0.14 s when the fault is cleared. At the time of the fault, the load currents achieve a peak value greater than 100 A because of the discharge of the capacitors. The use of these measurements in the overcurrent protection allows to maintain the peak currents injected by the VSC in a value lower than 40 A. Thus, the short circuit currents do not exceed the rated current of the VSC avoiding to damage the device. Note that both currents are stabilized in a time range less than 4 ms.

During the fault the voltages are practically zero. Once the fault is cleared, the voltages increase progressively according to the voltage drop (D4) shown in Fig. 3. The rated voltage references are restored when the current $\mathbf{i}_{s,abc}$ is lower than

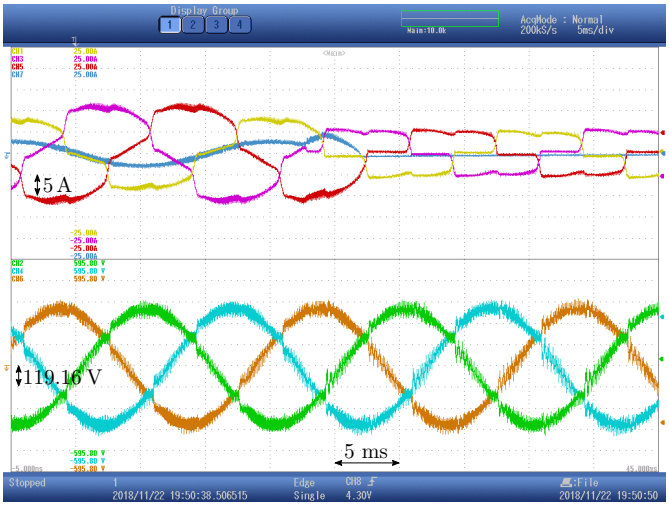

Fig. 12. Transient-state from *Test 3* to *Test 4*. Top: $i_{s,a}$ (yellow), $i_{s,b}$ (purple), $i_{s,c}$ (red) and $i_{s,n}$ (blue). Bottom: $v_{s,an}$ (green), $v_{s,bn}$ (light blue) and $v_{s,cn}$ (orange).

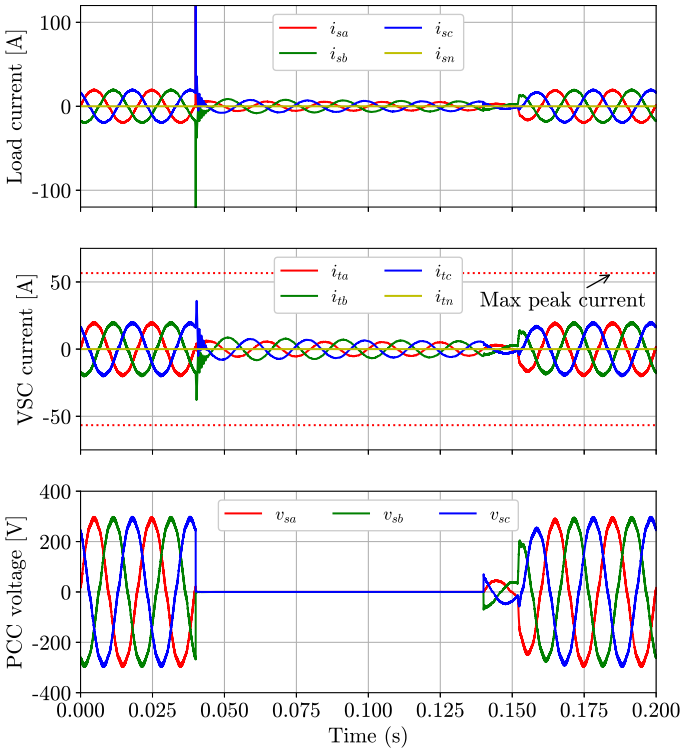

Fig. 13. HIL simulation of three-phase fault at PCC.

0.2 p.u. This restoration process takes about half a cycle of the fundamental frequency.

Note that if the overcurrent protection would have used $\mathbf{i}_{t,abc}$, the response time of this protection would have been delayed because this current does not reach so extremely high values. This would lead to an overcurrent situation for longer and could damage the VSC.

V. Conclusions

A novel control approach for grid-forming 4LVSC with an interconnection LC-filter has been presented in this paper. The objective is to establish a balanced three-phase voltage at the PCC under the presence of any type of load. To achieve it, a full state feedback law was applied on a dynamic extended model for the voltage control. In addition, a systematic methodology to compute the controller gains by solving an LQR problem subject to the extended system is presented. Thus, small signal system stability is ensured while offering active damping.

A Luenberger observer was developed to estimate the states of the plant obtaining greater robustness against noise. Moreover, an overcurrent protection has been included in the control algorithm in case of exceeding the rated current of the VSC.

The proposal was experimentally validated in a laboratory testbed through several test cases which have been evaluated using the limits defined of THDs and imbalances in the UNE-EN 50160 standard. The results show that the control algorithm obtains zero error in steady-state obtaining balanced voltages for any type of load as well as high robustness and fast transient response. The performance of the controller was compared with the classical cascade controller obtaining better values of the indexes analyzed in the presence of nonlinear loads. Finally, the control was evaluated in the presence of a three-phase fault demonstrating the effectiveness of the proposed overcurrent protection and justifying the advantage of measuring the current injected into the PCC.

References

[1] R. H. Lasseter, "Microgrids," in *2002 IEEE Power Engineering Society Winter Meeting. Conference Proceedings (Cat. No.02CH37309)*, vol. 1, pp. 305–308 vol.1, Jan 2002.

[2] D. E. Olivares, A. Mehrizi-Sani, A. H. Etemadi, C. A. Cañizares, R. Iravani, M. Kazerani, A. H. Hajimiragha, O. Gomis-Bellmunt, M. Saeedifard, R. Palma-Behnke, G. A. Jiménez-Estévez, and N. D. Hatziargyriou, "Trends in microgrid control," *IEEE Transactions on Smart Grid*, vol. 5, pp. 1905–1919, July 2014.

[3] J. M. Guerrero, J. C. Vasquez, J. Matas, L. G. de Vicuna, and M. Castilla, "Hierarchical control of droop-controlled ac and dc microgrids—a general approach toward standardization," *IEEE Transactions on Industrial Electronics*, vol. 58, pp. 158–172, Jan 2011.

[4] N. H. , *Microgrids: Architectures and Control*. John Wiley and Sons.

[5] I. Ziari, G. Ledwich, A. Ghosh, and G. Platt, "Integrated distribution systems planning to improve reliability under load growth," *IEEE Transactions on Power Delivery*, vol. 27, no. 2, pp. 757–765, 2012.

[6] J. A. Martinez, V. Dinavahi, M. H. Nehrir, and X. Guillaud, "Tools for analysis and design of distributed resources-Part IV: Future trends," *IEEE Transactions on Power Delivery*, vol. 26, no. 3, pp. 1671–1680, 2011.

[7] S. H. Ko, S. R. Lee, H. Dehbonei, and C. V. Nayar, "Application of voltage- and current-controlled voltage source inverters for distributed generation systems," *IEEE Transactions on Energy Conversion*, vol. 21, no. 3, pp. 782–792, 2006.

[8] N. A. Ninad and L. A. Lopes, "Per-phase vector (dq) controlled three-phase grid-forming inverter for stand-alone systems," *Proceedings - ISIE 2011: 2011 IEEE International Symposium on Industrial Electronics*, pp. 1626–1631, 2011.

[9] C. F. Nascimento, O. Diene, and E. H. Watanabe, "Analytical Model of Three-Phase Four-Wire VSC Operating as Grid-Forming Power Converter under Unbalanced Load Conditions," no. December, pp. 219–224, 2017.

[10] R. Lliuyacc, J. M. Mauricio, A. Gomez-Exposito, M. Savaghebi, and J. M. Guerrero, "Grid-forming VSC control in four-wire systems with unbalanced nonlinear loads," *Electric Power Systems Research*, vol. 152, pp. 249–256, 2017.

[11] J.-C. Wu, H.-L. Jou, K.-D. Wu, and H.-H. Hsiao, "Three-phase four-wire hybrid power filter using a smaller power converter," *Electric Power Systems Research*, vol. 87, pp. 13 – 21, 2012.

[12] S. Kumar and B. Singh, "Control of 4-leg vsc based dstatcom using modified instantaneous symmetrical component theory," in *2009 International Conference on Power Systems*, pp. 1–6, Dec 2009.

[13] J. Rocabert, A. Luna, F. Blaabjerg, and P. Rodríguez, "Control of power converters in AC microgrids," *IEEE Transactions on Power Electronics*, vol. 27, no. 11, pp. 4734–4749, 2012.

[14] M. K. Mishra, A. Ghosh, A. Joshi, and H. M. Suryawanshi, "A novel method of load compensation under unbalanced and distorted voltages," *IEEE Transactions on Power Delivery*, vol. 22, no. 1, pp. 288–295, 2007.

[15] B. Blažič and I. Papič, "Improved D-Statcom control for operation with unbalanced currents and voltages," *IEEE Transactions on Power Delivery*, vol. 21, no. 1, pp. 225–233, 2006.

[16] A. Yazdani and R. Iravani, "A unified dynamic model and control for the voltage-sourced converter under unbalanced grid conditions," *IEEE Transactions on Power Delivery*, vol. 21, no. 3, pp. 1620–1629, 2006.

[17] J. Hu and Y. He, "Modeling and control of grid-connected voltage-sourced converters under generalized unbalanced operation conditions," *IEEE Transactions on Energy Conversion*, vol. 23, no. 3, pp. 903–913, 2008.

[18] K. Li, J. Liu, Z. Wang, and B. Wei, "Strategies and operating point optimization of STATCOM control for voltage unbalance mitigation in three-phase three-wire systems," *IEEE Transactions on Power Delivery*, vol. 22, no. 1, pp. 413–422, 2007.

[19] A. K. Jain, K. Joshi, A. Behal, and N. Mohan, "Voltage regulation with STATCOMs: Modeling, control and results," *IEEE Transactions on Power Delivery*, vol. 21, no. 2, pp. 726–735, 2006.

[20] Y. Suh and T. A. Lipo, "Modeling and analysis of instantaneous active and reactive power for PWM AC/DC converter under generalized unbalanced network," *IEEE Transactions on Power Delivery*, vol. 21, no. 3, pp. 1530–1540, 2006.

[21] C. Hochgraf and R. H. Lasseter, "Statcom controls for operation with unbalanced voltages," *IEEE Transactions on Power Delivery*, vol. 13, no. 2, pp. 538–544, 1998.

[22] M. A. Torres L., L. A. Lopes, L. A. Moran T., and J. R. Espinoza C., "Self-Tuning Virtual Synchronous Machine: A Control Strategy for Energy Storage Systems to Support Dynamic Frequency Control," *IEEE Transactions on Energy Conversion*, vol. 29, no. 4, pp. 833–840, 2014.

[23] Y. Cao, W. Wang, Y. Li, Y. Tan, C. Chen, L. He, U. Häger, and C. Rehtanz, "A Virtual Synchronous Generator Control Strategy for VSC-MTDC Systems," *IEEE Transactions on Energy Conversion*, vol. 33, no. 2, pp. 750–761, 2018.

[24] K. De Brabandere, B. Bolsens, J. Van den Keybus, A. Woyte, J. Driesen, and R. Belmans, "A voltage and frequency droop control method for parallel inverters," *IEEE Transactions on Power Electronics*, vol. 22, pp. 1107–1115, July 2007.

[25] B. Singh and G. K. Kasal, "Voltage and frequency controller for a three-phase four-wire autonomous wind energy conversion system," *IEEE Transactions on Energy Conversion*, vol. 23, no. 2, pp. 509–518, 2008.

[26] I. Vechiu, H. Camblong, G. Tapia, B. Dakyo, and O. Curea, "Control of four leg inverter for hybrid power system applications with unbalanced load," *Energy Conversion and Management*, vol. 48, no. 7, pp. 2119–2128, 2007.

[27] N. A. Ninad and L. A. Lopes, "Unbalanced operation of per-phase vector controlled four-leg grid forming inverter for stand-alone hybrid systems," *IECON Proceedings (Industrial Electronics Conference)*, pp. 3500–3505, 2012.

[28] I. Vechiu, O. Curea, and H. Camblong, "Transient operation of a four-leg inverter for autonomous applications with unbalanced load," *IEEE Transactions on Power Electronics*, vol. 25, no. 2, pp. 399–407, 2010.

[29] Y. Han, P. Shen, X. Zhao, and J. M. Guerrero, "An Enhanced Power Sharing Scheme for Voltage Unbalance and Harmonics Compensation in an Islanded AC Microgrid," *IEEE Transactions on Energy Conversion*, vol. 31, pp. 1037–1050, sep 2016.

[30] P. Rodriguez, A. Luna, I. Candela, R. Mujal, R. Teodorescu, and F. Blaabjerg, "Multiresonant frequency-locked loop for grid synchronization of power converters under distorted grid conditions," *IEEE Transactions on Industrial Electronics*, vol. 58, pp. 127–138, Jan 2011.

[31] K. Ogata, *Modern control engineering*. Englewood Cliffs, N.J: Prentice-Hall, 2nd ed. ed., 1990.

[32] D. Luenberger, "An introduction to observers," *IEEE Transactions on Automatic Control*, vol. 16, pp. 596–602, December 1971.

[33] B. Francis and W. Wonham, "The internal model principle of control theory," *Automatica*, vol. 12, no. 5, pp. 457 – 465, 1976.

[34] M. A. Johnson and M. J. Grimble, "Recent trends in linear optimal quadratic multivariable control system design," *IEE Proceedings D - Control Theory and Applications*, vol. 134, pp. 53–71, January 1987.
[35] R. Zhang, V. H. Prasad, D. Boroyevich, and F. C. Lee, "Three-dimensional space vector modulation for four-leg voltage-source converters," *IEEE Transactions on Power Electronics*, vol. 17, no. 3, pp. 314–326, 2002.

Juan Carlos Olives-Camps was born in Menorca, Spain, in 1991. He received the degree from the Technical University of Catalonia (UPC), Barcelona, Spain, in 2014, and the Master's degree from University of Seville, Seville, Spain, in 2018, both in electrical engineering. He is currently working toward the Ph.D. degree at the Department of Electrical Engineering, University of Seville. His primary areas of interest include power systems control, voltage source converters-based applications, and renewable energy integration.

Juan Manuel Mauricio was born in Argentina in 1977. He received the degree in electrical engineering from the National University of Comahue, Neuquen, Argentina, in 2003, and the Master's and Dr. Eng. degrees from the University of Seville, Seville, Spain, in 2007 and 2009, respectively. Since 2004, he has been with the Department of Electrical Engineering, University of Seville, where he is currently an Assistant Professor. His primary research interests include power systems and electrical machine control, renewable generation, voltage source converters-based applications, and electrical vehicles.

Manuel Barragán-Villarejo was born in Spain in 1984. He received the Electrical Engineering and Ph.D. degrees in electrical engineering from the University of Seville, Seville, Spain, in 2008 and 2014, respectively. Since 2008, he has been with the Department of Electrical Engineering, University of Seville, where he is currently an Assistant Professor. His primary research interests include exploitation of new power converter topologies for smart grid management and grid integration of renewable energy resources.

Francisco Jesús Matas-Díaz was born in Spain in 1995. He received the aerospace engineering degree from the University of Seville, Seville, Spain, in 2017, where he is currently a research assistant at the Department of Electrical Engineering. His primary areas of interest are microcontrollers programming, HIL simulations and power converters experimental validation.